Biodistribution and Radiation Dosimetry of ^{18}F-FTC-146 in Humans

Trine Hjørnevik[1–3], Peter W. Cipriano[1], Bin Shen[1], Jun Hyung Park[1], Praveen Gulaka[1], Dawn Holley[1], Harsh Gandhi[1], Daehyun Yoon[1], Erik S. Mittra[1], Greg Zaharchuk[1], Sanjiv S. Gambhir[1], Christopher R. McCurdy[4,5], Frederick T. Chin[1], and Sandip Biswal[1]

[1]Department of Radiology, Stanford University, Stanford, California; [2]Department of Diagnostic Physics, Oslo University Hospital, Oslo, Norway; [3]The Norwegian Medical Cyclotron Centre, Oslo, Norway; [4]Department of Medicinal Chemistry, University of Florida, Gainesville, Florida; and [5]UF Translational Drug Development Core, University of Florida, Gainesville, Florida

The purpose of this study was to assess safety, biodistribution, and radiation dosimetry in humans for the highly selective σ-1 receptor PET agent ^{18}F-6-(3-fluoropropyl)-3-(2-(azepan-1-yl)ethyl)benzo[d]thiazol-2(3H)-one (^{18}F-FTC-146). **Methods:** Ten healthy volunteers (5 women, 5 men; age ± SD, 34.3 ± 6.5 y) were recruited, and written informed consent was obtained from all participants. Series of whole-body PET/MRI examinations were acquired for up to 3 h after injection (357.2 ± 48.8 MBq). Blood samples were collected, and standard vital signs (heart rate, pulse oximetry, and body temperature) were monitored at regular intervals. Regions of interest were delineated, time–activity curves were calculated, and organ uptake and dosimetry were estimated. **Results:** All subjects tolerated the PET/MRI examination well, and no adverse reactions to ^{18}F-FTC-146 were reported. High accumulation of ^{18}F-FTC-146 was observed in σ-1 receptor–dense organs such as the pancreas and spleen, moderate uptake in the brain and myocardium, and low uptake in bone and muscle. High uptake was also observed in the kidneys and bladder, indicating renal tracer clearance. The effective dose of ^{18}F-FTC-146 was 0.0259 ± 0.0034 mSv/MBq (range, 0.0215–0.0301 mSv/MBq). **Conclusion:** First-in-human studies with clinical-grade ^{18}F-FTC-146 were successful. Injection of ^{18}F-FTC-146 is safe, and absorbed doses are acceptable. The potential of ^{18}F-FTC-146 as an imaging agent for a variety of neuroinflammatory diseases is currently under investigation.

Key Words: sigma-1 receptor; radiation dosimetry; biodistribution; first-in-human; PET

S igma-1 receptors (S1Rs), a unique class of intercellular chaperone proteins, are widely distributed in the central nervous system and peripheral tissues. S1Rs modulate ion channels and other neurotransmitter systems, and are therefore involved in many biologic mechanisms associated with pain, inflammation, neuronal protection, neurodegeneration, cancer, addiction, and psychiatric diseases.

S1Rs are expressed in both neurons and glial cells and are believed to have an important role in preserving and restoring neuronal function. Study of S1Rs may provide important insight into degenerative disorders such as Alzheimer disease, stroke, Parkinson disease, and amyotrophic lateral sclerosis (*1*). Prior studies suggest a strong link between S1Rs and important brain functions such as mood and cognition (*2,3*). In particular, stimulation of S1Rs dampened depression-like behavior in mice (*4*). Several studies have indicated that S1Rs also play a key role in nociception (*5–7*) and are known to interact with opioid receptors and modulate opioid activity (*8,9*). In particular, antinociceptive effects of S1R antagonists both when acting alone and in combination with opioids (to enhance opioid analgesia) have been reported at both central and peripheral sites (*8,9*). Emerging evidence for the involvement of S1Rs in various diseases makes the S1R a promising biomarker for research in diagnostic imaging and therapy.

PET is a highly sensitive imaging modality that uses specifically designed radioligands to quantify molecular processes in vivo. Several groups have developed S1R-targeting radioligands with different pharmacophore structures, such as piperazines (*10*) and piperidines (*11*). However, only 3 compounds have thus far been used in clinical studies: ^{11}C-SA4503 (inhibition constant [K_i] = 4.6 nM (*12*)), ^{18}F-FPS (K_i = 4.3 nM (*13,14*)), and ^{18}F-fluspidine (K_i = 0.59 nM (*15*)). ^{11}C-SA4503 displays significant affinity for the σ-2 receptor (K_i = 63 nM (*16*)) and vesicular acetylcholine transporters (K_i = 50 nM (*17*)); these interactions may confound imaging results when specifically interrogating for S1R. ^{18}F-FPS has shown unfavorable slow brain pharmacokinetics, which limits the clinical evaluation of S1Rs in the central nervous system. Recently, ^{18}F-fluspidine has been tested in healthy human subjects (*18*), and further clinical application is pending.

Since 2011, our group has been developing a highly selective S1R radioligand, ^{18}F-FTC-146 (Fig. 1). The excellent selectivity (>1,000-fold) for the S1R over the σ-2 receptor and vesicular acetylcholine transporters demonstrates the high potential of ^{18}F-FTC-146 for selectively imaging the S1R. Preclinical studies (i.e., cell line, wild-type and S1R knock-out mice, rats, and nonhuman primates) of ^{18}F-FTC-146 have shown excellent pharmacokinetic imaging properties and biosafety (*19–21*). On the basis of these favorable preclinical findings, we obtained exploratory
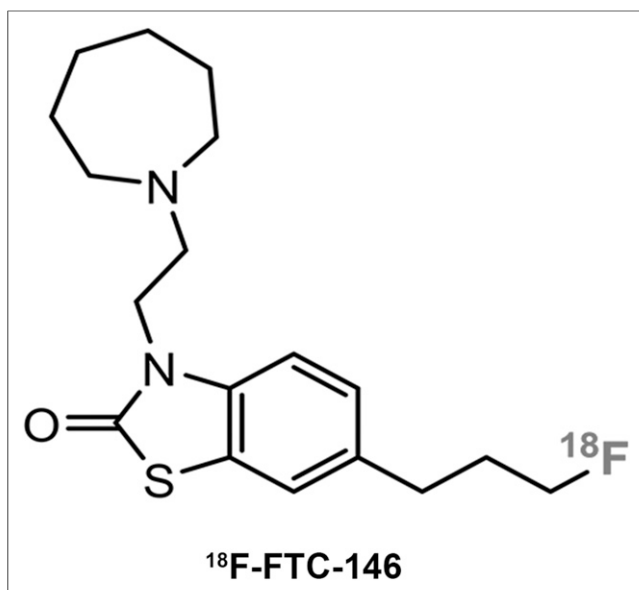
FIGURE 1. Chemical structure of ^{18}F-FTC-146.

Investigational New Drug status for clinical-grade ^{18}F-FTC-146 to allow first-in-human ^{18}F-FTC-146 studies (*22*).

The purpose of this study was to assess the safety, biodistribution, and radiation dosimetry for clinical-grade ^{18}F-FTC-146 in humans.

MATERIALS AND METHODS

Subjects

The study protocol was approved by the Stanford University Institutional Review Board and is compliant with federal, state, and local regulation on medical research (clinical trial registration no. NCT02753101). Ten healthy volunteers (5 women, 5 men; age, 34.3 ± 6.5 y) were recruited between February and April 2016 (Table 1), and written informed consent was obtained from each subject before commencing the study. Inclusion criteria were adults 18–50 y of age. Exclusion criteria included pregnancy, breastfeeding, MRI-incompatible materials and devices, and presence of pain, which was assessed using the Oswestry Disability Index, visual analog scale, and Short Form 36 Health Survey.

No specific patient preparation was requested (i.e., fasting or hydration) on the day of scanning. The volunteer's vital signs (heart rate, pulse oximetry, and body temperature) were monitored at regular intervals throughout the duration of imaging. To determine whether the injected dose of ^{18}F-FTC-146 affected blood measurements over time, blood specimens were obtained and analyzed (complete blood count with differential, renal function panel, and liver function panel) from each volunteer at 3 time points: immediately before the injection of ^{18}F-FTC-146; 24 h after injection of ^{18}F-FTC-146; and 7 d after injection of ^{18}F-FTC-146. Any unusual or adverse patient symptoms were recorded on the day of imaging as well as during follow-up.

Radiosynthesis

In-depth details regarding the synthesis and quality control of clinical-grade ^{18}F-FTC-146 are published elsewhere (*22*). In brief, ^{18}F-FTC-146 was synthesized via aliphatic nucleophilic substitution (^{18}F/tosylate exchange) using TRACERlab FX-FN. Tosylate precursor solution (2.5 mg in 1 mL of anhydrous dimethyl sulfoxide) was added into azeotropically dried ^{18}F/K$_{222}$/K$_2$CO$_3$ complex and heated to 150°C for 15 min, and the crude product was purified on semipreparative high-performance liquid chromatography. The ^{18}F-FTC-146 high-performance liquid chromatography fraction was formulated in saline containing no more than 10% ethanol. The specific activity at the end of bombardment was 173.9 ± 66.6 GBq/μmol.

PET Imaging and Reconstruction

The mean and SD of the administered mass and activity of ^{18}F-FTC-146 was 1.4 ± 0.5 μg (range, 0.57–2.44 μg) and 357.2 ± 48.8 MBq (range, 269.0–419.2 MBq), respectively. All subjects underwent a series of PET/MR examinations scheduled at 0, 30, 60, 90, 120, 150, and 180 min after tracer administration on a time-of-flight PET/MR scanner (SIGNA PET/MR; GE Healthcare).

The first PET/MR examination started simultaneously with tracer administration and consisted of a 10-min acquisition of the brain, followed by a whole-body (WB) PET/MR scan. Data were acquired for at least 6 bed positions with 2-min PET acquisitions per bed together with simultaneous MRI scans (T1- and T2-weighted images) for anatomic reference and attenuation correction (2-point Dixon sequence). The PET photon attenuation coefficients at 511 keV were obtained by segmenting the MR-based attenuation correction images into air, lung, fat, and water (everywhere except the brain), which was registered to an atlas containing skull information.

For the first 5 subjects, WB scans covering the head to mid thigh were obtained, whereas for subjects 6–10, additional total-body scans (head to toe) were acquired at 3 time points (Table 2). The PET data were reconstructed using a fully 3-dimensional iterative ordered-subsets expectation maximization algorithm (28 subsets, 2 iterations) and corrected for attenuation, scatter, dead time, and decay. Subjects were allowed to momentarily leave the scanner after the 30-min scan and were strongly encouraged to void their bladder.

Biodistribution and Radiation Dosimetry

Organs of interest (kidneys, brain, liver, pancreas, spleen, thyroid, urinary bladder, muscle, cortical bone, heart wall, brain, and marrow) were delineated using PMOD 3.7 (PMOD Technologies LLC), and the corresponding SUVs were calculated for each imaging time point. In addition, to estimate the total number of disintegrations (residence

TABLE 1
Subject Demographics and Administered ^{18}F-FTC-146 Dose Data

HV no.	Sex	Age (y)	Height (cm)	Weight (kg)	Injected activity (MBq)
1	M	33	175.3	103.4	307.8
2	F	41	162.6	61.2	346.3
3	F	35	170.2	78.0	269.0
4	M	29	174.0	70.0	405.5
5	M	28	178.0	80.0	342.3
6	M	31	170.2	68.0	371.5
7	F	36	165.1	54.4	325.6
8	M	33	177.8	100.0	414.8
9	F	28	162.6	63.5	419.2
10	F	49	167.6	79.4	370.0
Mean		34.3	170.3	75.8	357.2
SD		6.5	5.8	16.0	48.8

HV = healthy volunteer.

TABLE 2
^{18}F-FTC-146 Imaging Protocol

| HV no. | Start time after tracer injection for each PET/MR scan (min) | | | | | | | No. of WB* PET/MR scans |
	0	30	60	90	120	150	180	
1	0	43		85	122			4
2	0	35	77	100	127			5
3	0	43		101	126			4
4	0	34	69	93	123			5
5	0	38	78	104	125			5
6	0	33†	76†		115	132†	172	6
7	0	31†	74†	102	126†	154		6
8	0	31†		80†	115	136†	172	6
9	0	32†	73†	100	129†	160		6
10	0	29†		78†	117	139†		5
Mean	0	34.9	74.5	93.7	122.5	144.2	172.0	5.2
SD	0	4.9	3.3	10.1	5.1	12.1	0.0	0.8

*Head to mid thigh scan coverage.

†Total-body (head to toe) scan coverage.

HV = healthy volunteer.

Actual imaging start time points (minutes after tracer administration) and number of WB PET/scans for each volunteer.

times in hours) in each organ, the total organ uptake was calculated on the basis of the average (non–decay-corrected) concentration data and standardized phantom organ volumes as implemented in PMOD 3.7. To avoid any underestimation of absorbed doses, the activity was normalized to account for 100% of the injected activity. The activity data were fitted by trapezoidal integration to the end of scanning, followed by isotope decay. The resulting residence times were imported to OLINDA/EXM software (23) for radiation dose estimations. The remainder in the body was calculated by subtracting the sum of the activity in all source organs from the total activity in the body. The total number of integrations for the bladder was determined using the urinary bladder model as implemented in OLINDA/EXM, with a 1-h bladder-voiding interval and 100% renal excretion. The biologic half-life of ^{18}F-FTC-146 was estimated from the WB activity data. The phantoms selected in OLINDA/EXM were the adult female and male phantoms, for female and male subjects, respectively. In addition, to allow for individual variations in organ mass, the phantom organ volumes were scaled according to the subject's individual body weight as implemented in OLINDA/EXM. The effective dose (ED) was determined using the methodology defined in International Commission on Radiological Protection publication 60 (24).

RESULTS

All subjects tolerated the PET/MRI examination well. No adverse reactions to ^{18}F-FTC-146 were reported during the day of scanning or during the 7-d follow-up period. As required by the Food and Drug Administration, a full assessment including blood pressure and blood count were performed for acute toxicity assessment, and no abnormal findings were observed. Subject 8 disclosed, after the end of scanning, low-grade muscle soreness due to performing intense exercise the day before. Hence, because subject 8 was not an asymptomatic volunteer, subject 8's results were eliminated from the biodistribution and dosimetry assessment.

All subjects were scheduled to be scanned at 30-min intervals for up to 3 h after tracer administration. However, the start time of each WB scan and the number of scans varied slightly between subjects because of logistics and patient comfort. In particular, the 60-min WB was often delayed because of the encouraged bathroom break. The exact timing of the WB scans and total number of scans for the individual subjects are listed in Table 2.

^{18}F-FTC-146 Biodistribution and Dosimetry

Figure 2 shows the uptake pattern and biodistribution of ^{18}F-FTC-146 at 6 different time points after tracer administration in a healthy volunteer (subject 7; Fig. 2A) as well as the intersubject variability between volunteers (n = 9) at 30 min after tracer administration (Fig. 2B). The corresponding coronal and axial PET/MR images in Figure 3 show tracer distribution in several key areas of the body (subject 10). High accumulation of ^{18}F-FTC-146 was observed in S1R-dense organs such as the pancreas, spleen, and thyroid, whereas moderate uptake was observed in the brain and myocardium, and low uptake in bone and muscle. Renal tracer clearance resulted in the expectedly high uptake observed in the kidneys and bladder. High accumulation of ^{18}F-FTC-146 was also observed in the veins of the arm on the side of injection (Fig. 2). Figure 4 shows the average (n = 9) time–activity curves for 10 principal organs; the reported SUVs are corrected for physical decay. A gradual tracer washout was observed in the lungs, kidneys, and bladder.

The absorbed dose estimates for the 9 included participants are listed in Table 3. The bladder received the highest dose of all organs (0.1498 ± 0.0245 mSv/MBq), reflecting renal tracer clearance. The other
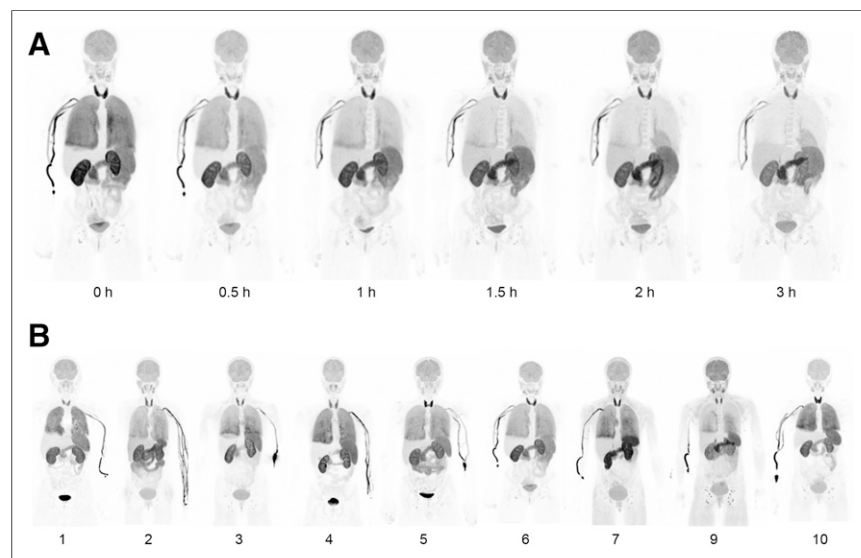

FIGURE 2. WB PET maximum-intensity-projection images at different time points after ^{18}F-FTC-146 administration in subject 7 (A) and at 30 min after ^{18}F-FTC-146 administration in 9 subjects (B).
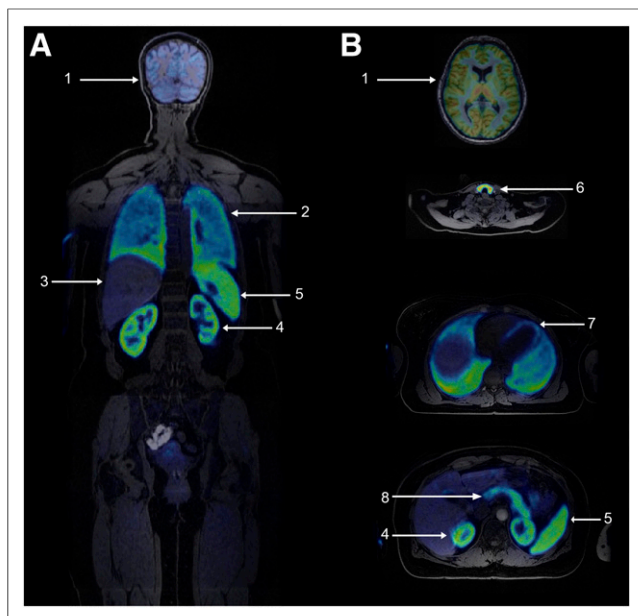
FIGURE 3. Simultaneous PET/MRI in coronal (A) and transverse (B) planes showing uptake in principal organs 30 min after ^{18}F-FTC-146 injection in subject 10: brain (1), lungs (2), liver (3), kidneys (4), spleen (5), thyroid (6), heart (7), and pancreas (8).

major organs that received relatively high doses were the pancreas (0.0654 ± 0.0208 mSv/MBq), spleen (0.0637 ± 0.0117 mSv/MBq), kidneys (0.0577 ± 0.0080 mSv/MBq), and thyroid (0.0457 ± 0.0100 mSv/MBq). The thymus, testes, skin, marrow, ovaries, breasts, and adrenals received the lowest absorbed doses. The highest intersubject variation in absorbed dose was observed in the bladder (range, 0.1230–0.1710 mSv/MBq) and pancreas (range, 0.0381–0.1100 mSv/MBq).

The mean ED of ^{18}F-FTC-146 was 0.0259 ± 0.0034 mSv/MBq (range, 0.0215–0.0301 mSv/MBq). With an injected ^{18}F-FTC-146

dose of 370 MBq and a 1-h voiding interval, the patient would be exposed to an ED of 9.6 mSv. After correcting for body weight, the mean ED was 0.0245 ± 0.0034 mSv/MBq (range, 0.0177–0.0296 mSv/MBq), and the patient radiation exposure from ^{18}F-FTC-146 was 9.1 mSv.

DISCUSSION

This first-in-human PET/MRI study demonstrates the safety, biodistribution, and radiation dosimetry of clinical-grade ^{18}F-FTC-146. Multiple WB PET/MRI scans were obtained successfully in 10 volunteers, and no adverse reaction or clinical changes in vital signs were observed. The estimated absorbed doses to critical and radiation-sensitive organs are acceptable and considered to be safe.

The organs showing primary uptake of ^{18}F-FTC-146 are those known to have a high expression of S1R (25,26), such as the spleen, pancreas, heart wall, brain, normal groin and axillary lymph nodes, thyroid, and lungs. The primary route of tracer clearance was through the renal pathway, resulting in high uptake and gradual washout in the kidneys and bladder. Although uptake was also observed in the small intestine, we believe that this accumulation occurred in the Peyer's patches of the small bowel's lymph node system. In addition, no uptake was observed in the gallbladder or in the colon over time. Hence, we concluded that the tracer excretes solely through the renal and not the hepatobiliary pathway.

A full assessment of radiometabolites from ^{18}F-FTC-146 administration in human plasma has been previously published (22). In brief, 43% ± 7% and 23% ± 5% of the peak radioactivity remained in circulation at 30 and 120 min after injection, respectively. On the basis of our preclinical studies, only intact ^{18}F-FTC-146 was present in the rat brain at 15, 30, and 60 min after injection (19).

In contrast to tracer uptake in the skull observed in our previous nonhuman primate study (19), only insignificant radioactivity uptake in bone was detected in humans. Also, differences in tracer pharmacokinetic properties were observed between the 2 species; slow tracer washout was seen in monkeys unlike in human brain tissue in which no gradual washout of ^{18}F-FTC-146 was detected within the 3-h imaging session. The observed slower kinetics are likely due to high S1R binding affinity in the picomolar range. Although slow tracer kinetics are not ideal for a neuroimaging probe, they facilitate high signal-to-background contrast, enabling potential detection of smaller foci related to disease, such as pain and nerve injury. In addition, high specific binding provides advantages for future translation of S1R-specific therapeutic strategies.

^{18}F-FTC-146 was retained in the veins of the arm that was injected, a phenomenon also observed in a recent human study with ^{18}F-fluspidine (18). To prevent this radiotracer retention in the vein, we are working to improve the tracer's solubility under physiologic conditions by experimenting with different formulation strategies. No specific dosimetric assessment was conducted on the basis of this uptake; the amount of
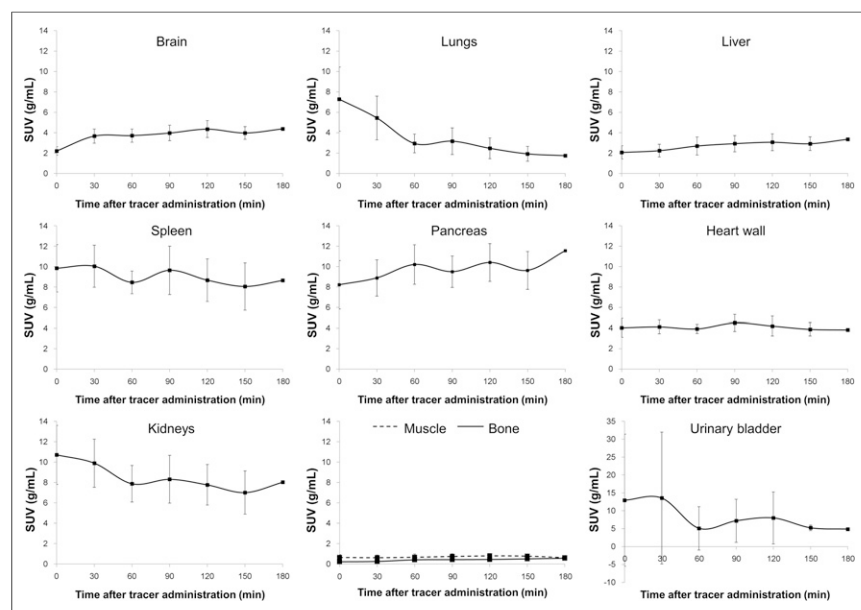

FIGURE 4. Average (n = 9) time–activity curves for 10 principal organs. Error bars indicate ± SD. SUVs at 180 min are based on a single subject only (no error bars). Note scale difference on y-axis for urinary bladder.

TABLE 3
^{18}F-FTC-146 Dosimetric Data

Target organ	Mean	SD	Minimum	Maximum
Adrenals	0.0161	0.0023	0.0133	0.0193
Brain	0.0307	0.0054	0.0218	0.0406
Breasts	0.0094	0.0012	0.0077	0.0111
Gallbladder wall	0.0166	0.0021	0.0140	0.0208
Lower large intestine wall	0.0171	0.0021	0.0131	0.0194
Small intestine	0.0318	0.0122	0.0125	0.0558
Stomach wall	0.0150	0.0018	0.0123	0.0172
Upper large intestine wall	0.0171	0.0025	0.0120	0.0200
Heart wall	0.0332	0.0075	0.0234	0.0436
Kidneys	0.0577	0.0080	0.0459	0.0717
Liver	0.0272	0.0087	0.0162	0.0480
Lungs	0.0262	0.0046	0.0215	0.0356
Muscle	0.0115	0.0026	0.0080	0.0154
Ovaries	0.0177	0.0021	0.0133	0.0195
Pancreas	0.0654	0.0208	0.0381	0.1100
Red marrow	0.0152	0.0022	0.0124	0.0198
Osteogenic cells	0.0207	0.0038	0.0160	0.0274
Skin	0.0082	0.0010	0.0067	0.0096
Spleen	0.0637	0.0117	0.0419	0.0785
Testes	0.0105	0.0006	0.0098	0.0113
Thymus	0.0117	0.0017	0.0094	0.0139
Thyroid	0.0457	0.0100	0.0275	0.0643
Urinary bladder wall	0.1498	0.0245	0.1230	0.1710
Uterus	0.0216	0.0021	0.0174	0.0234
Total body	0.0145	0.0020	0.0119	0.0163
Effective dose	0.0259	0.0034	0.0215	0.0301

Data are absorbed dose estimates (mSv/MBq).

tracer accumulation in the arm was included in the remainder of the body.

The estimated ED of ^{18}F-FTC-146 was 0.0259 ± 0.0034 mSv/MBq, with an uppermost estimated individual ED of 0.0301 mSv/MBq. An injected dose of 370 MBq will expose the patient to 9.6 mSv (based on mean) or 11.1 mSv (based on maximum). After correction for individual body weights, the highest radiation exposure was estimated to be 11.0 mSv. The estimated radiation doses are comparable to other ^{18}F-labeled radiopharmaceuticals (27), such as ^{18}F-FPPRGD2 (0.0396 ± 0.0181 mSv/MBq (28)) and the S1R radioligand ^{18}F-fluspidine (0.021 ± 0.013 mSv/MBq (18)). For comparison, radiation exposure from a standard ^{18}F-FDG PET examination is typically 6–7 mSv (27).

For radioactive agents used in clinical trials, dose limitations for adult research subjects are defined in the United States by the U.S. Food and Drug Administration (29). For blood-forming organs, lens of the eye, gonads, and WB, the radiation doses must not exceed 30 mSv per examination or 50 mSv per year. For all other organs, the limits for single and total annual dose are 50 and 150 mSv, respectively. On the basis of the calculated WB dosimetric values, 1,930 MBq of ^{18}F-FTC-146 can be injected in each patient per year, hence, 5 ^{18}F-FTC-146 PET acquisitions with 370 MBq can be conducted annually. For radiation-sensitive organs, such as the testes, ovaries, and red marrow, the dosimetric calculations show that the absorbed organ doses are well below the 30-mSv dose limit given by the Food and Drug Administration.

For the hybrid, WB PET/MR scanner, the MR-based attenuation-correction methodology does not include correction for photon attenuation in bone. Hence, measured activity values in the PET images may be underestimated for tissue surrounded by a substantial amount of bone. However, Iagaru et al. (30) demonstrated that the image quality was improved and the measured activity values were higher in PET images obtained with PET/MRI compared with PET/CT. Another study showed that the SUV based on PET/CT and PET/MRI correlated well in normal organ tissues, except for the lungs, subcutaneous fat, and blood pool (31). In addition, because of the high sensitivity of the current PET/MR scanner (32), we believe that the calculated ED values provide accurate estimates of the radiation exposure to patients.

^{18}F-FTC-146 is a promising imaging agent for a variety of applications, because SIRs are believed to play an important role in cancer, chronic pain, and neurologic disorders. We are currently investigating the potential of ^{18}F-FTC-146 to image pain generators in the peripheral nervous system. The high selectivity and affinity of the tracer facilitate an excellent signal-to-noise ratio, which is necessary for such small imaging targets.

CONCLUSION

First-in-human studies with clinical-glade ^{18}F-FTC-146 have been successful. Injection of ^{18}F-FTC-146 is safe, and absorbed doses are acceptable. The potential of ^{18}F-FTC-146 as an imaging agent for chronic pain and neuroinflammatory diseases is currently under investigation.

DISCLOSURE

ACKNOWLEDGMENTS

REFERENCES

1. Nguyen L, Lucke-Wold BP, Mookerjee SA, et al. Role of sigma-1 receptors in neurodegenerative diseases. *J Pharmacol Sci.* 2015;127:17–29.
2. Hayashi T, Su TP. Sigma-1 receptor ligands: potential in the treatment of neuropsychiatric disorders. *CNS Drugs.* 2004;18:269–284.
3. Fishback JA, Robson MJ, Xu YT, Matsumoto RR. Sigma receptors: potential targets for a new class of antidepressant drug. *Pharmacol Ther.* 2010;127:271–282.
4. Moriguchi S, Sakagami H, Yabuki Y, et al. Stimulation of sigma-1 receptor ameliorates depressive-like behaviors in CaMKIV null mice. *Mol Neurobiol.* 2015;52:1210–1222.

5. Almansa C, Vela JM. Selective sigma-1 receptor antagonists for the treatment of pain. *Future Med Chem.* 2014;6:1179–1199.

6. Davis MP. Sigma-1 receptors and animal studies centered on pain and analgesia. *Expert Opin Drug Discov.* 2015;10:885–900.

7. Gris G, Cobos EJ, Zamanillo D, Portillo-Salido E. Sigma-1 receptor and inflammatory pain. *Inflamm Res.* 2015;64:377–381.

8. Kim FJ, Kovalyshyn I, Burgman M, Neilan C, Chien CC, Pasternak GW. Sigma 1 receptor modulation of G-protein-coupled receptor signaling: potentiation of opioid transduction independent from receptor binding. *Mol Pharmacol.* 2010;77:695–703.

9. Vidal-Torres A, de la Puente B, Rocasalbas M, et al. Sigma-1 receptor antagonism as opioid adjuvant strategy: enhancement of opioid antinociception without increasing adverse effects. *Eur J Pharmacol.* 2013;711:63–72.

10. Kawamura K, Ishiwata K, Tajima H, et al. In vivo evaluation of [^{11}C]SA4503 as a PET ligand for mapping CNS sigma$_1$ receptors. *Nucl Med Biol.* 2000;27:255–261.

11. Waterhouse RN, Stabin MG, Page JG. Preclinical acute toxicity studies and rodent-based dosimetry estimates of the novel sigma-1 receptor radiotracer [^{18}F]FPS. *Nucl Med Biol.* 2003;30:555–563.

12. Lever JR, Gustafson JL, Xu R, Allmon RL, Lever SZ. Sigma1 and sigma2 receptor binding affinity and selectivity of SA4503 and fluoroethyl SA4503. *Synapse.* 2006;59:350–358.

13. Collier TL, O'Brien JC, Waterhouse RN. Synthesis of [~~F]-l-(3-FIuoropropyI)-4-(4-cyanophenoxymethyl)-piperidine: a potential sigma-1 receptor radioligand for PET. *J Labelled Comp Radiopharm.* 1996;38:785–794.

14. Waterhouse RN, Nobler MS, Zhou Y, et al. First evaluation of the sigma-1 receptor radioligand [^{18}F]1-fluoropropyl-4-((4-cyanophenoxy)-methyl)piperidine ([^{18}F]FPS) in humans. *Neuroimage.* 2004;22:T29–30.

15. Fischer S, Wiese C, Maestrup EG, et al. Molecular imaging of sigma receptors: synthesis and evaluation of the potent sigma1 selective radioligand [^{18}F]fluspidine. *Eur J Nucl Med Mol Imaging.* 2011;38:540–551.

16. Bhuiyan MS, Fukunaga K. Targeting sigma-1 receptor signaling by endogenous ligands for cardioprotection. *Expert Opin Ther Targets.* 2011;15:145–155.

17. Ishiwata K, Kawamura K, Yajima K. QingGeLeTu, Mori H, Shiba K. Evaluation of (+)-p-[^{11}C]methylvesamicol for mapping sigma1 receptors: a comparison with [^{11}C]SA4503. *Nucl Med Biol.* 2006;33:543–548.

18. Kranz M, Sattler B, Wust N, et al. Evaluation of the enantiomer specific biokinetics and radiation doses of [^{18}F]fluspidine: a new tracer in clinical translation for imaging of sigma$_1$ receptors. *Molecules.* 2016;21:pii: E1164.

19. James ML, Shen B, Nielsen CH, et al. Evaluation of sigma-1 receptor radioligand ^{18}F-FTC-146 in rats and squirrel monkeys using PET. *J Nucl Med.* 2014;55:147–153.

20. James ML, Shen B, Zavaleta CL, et al. New positron emission tomography (PET) radioligand for imaging sigma-1 receptors in living subjects. *J Med Chem.* 2012;55:8272–8282.

21. Shen B, James ML, Andrews L, et al. Further validation to support clinical translation of [^{18}F]FTC-146 for imaging sigma-1 receptors. *EJNMMI Res.* 2015;5:49.

22. Shen B, Park JH, Hjornevik T, et al. Radiosynthesis and first-in-human PET/MRI evaluation with clinical-grade [^{18}F]FTC-146. *Mol Imaging Biol.* March 9, 2017 [Epub ahead of print].

23. Stabin MG, Sparks RB, Crowe E. OLINDA/EXM: the second-generation personal computer software for internal dose assessment in nuclear medicine. *J Nucl Med.* 2005;46:1023–1027.

24. Protection ICoR. *1990 Recommendations of the International Commission on Radiological Protection.* ICRP publication 60. New York: Pergamon Press; 1991.

25. Romero L, Merlos M, Vela JM. Chapter seven: antinociception by sigma-1 receptor antagonists—central and peripheral effects. In: James EB, ed. *Advances in Pharmacology.* Vol. 75. Cambridge, MA: Academic Press; 2016:179–215.

26. Uhlén M, Fagerberg L, Hallstrom BM, et al. Proteomics: tissue-based map of the human proteome. *Science.* 2015;347:1260419.

27. Protection ICoR. *Radiation Dose to Patients from Radiopharmaceuticals (Addendum to ICRP publication 53).* New York, NY: Pergamon Press; 1998.

28. Mittra ES, Goris ML, Iagaru AH, et al. Pilot pharmacokinetic and dosimetric studies of ^{18}F-FPPRGD2: a PET radiopharmaceutical agent for imaging $\alpha_v\beta_3$ integrin levels. *Radiology.* 2011;260:182–191.

29. §361.1 Radioactive drugs for certain research uses. U.S. Food and Drug Administration website. https://www.ecfr.gov/cgi-bin/text-idx?SID=50764b2c150513d096625541cc556b76&mc=true&node=pt21.5.361&rgn=div5. Updated April 25, 2017. Accessed August 2, 2017.

30. Iagaru A, Mittra E, Minamimoto R, et al. Simultaneous whole-body time-of-flight ^{18}F-FDG PET/MRI: a pilot study comparing SUVmax with PET/CT and assessment of MR image quality. *Clin Nucl Med.* 2015;40:1–8.

31. Heusch P, Buchbender C, Beiderwellen K, et al. Standardized uptake values for [^{18}F] FDG in normal organ tissues: comparison of whole-body PET/CT and PET/MRI. *Eur J Radiol.* 2013;82:870–876.

32. Grant AM, Deller TW, Khalighi MM, Maramraju SH, Delso G, Levin CS. NEMA NU 2-2012 performance studies for the SiPM-based ToF-PET component of the GE SIGNA PET/MR system. *Med Phys.* 2016;43:2334–2343.